PCCP

PAPER

View Article Online
View Journal | View Issue

Cite this: *Phys. Chem. Chem. Phys.*, 2020, **22**, 24697

Na_2CO_3-modified CaO-based CO_2 sorbents: the effects of structure and morphology on CO_2 uptake†

Alexey Kurlov, [a] Agnieszka M. Kierzkowska, [a] Thomas Huthwelker, [b] Paula M. Abdala *[a] and Christoph R. Müller *[a]

Calcium looping (CaL) is a CO_2 capture technique based on the reversible carbonation/calcination of CaO that is considered promising to reduce anthropogenic CO_2 emissions. However, the rapid decay of the CO_2 uptake of CaO over repeated cycles of carbonation and calcination due to sintering limits its implementation at the industrial scale. Thus, the development of material design strategies to stabilize the CO_2 uptake capacity of CaO is paramount. The addition of alkali metal salts to CaO has been proposed as a strategy to mitigate the rapid loss of its cyclic CO_2 uptake capacity. However, there are conflicting results concerning the effect of the addition of alkali metal carbonates on the structure and CO_2 capacity of CaO. In this work, we aim at understanding the effect of the addition of Na_2CO_3 to CaO on the sorbent's structure and its CO_2 uptake capacity. We demonstrate that under industrially-relevant conditions the addition of as little as 1 wt% of Na_2CO_3 reduces severely the CO_2 uptake of CaO. Combining TGA, XAS and FIB-SEM analysis allowed us to attribute the performance degradation to the formation of the double salt $Na_2Ca(CO_3)_2$ that induces strong sintering leading to a significant loss in the sorbent's pore volume. In addition, during the carbonation step the formation of a dense layer of $Na_2Ca(CO_3)_2$ that covers unreacted CaO prevents its full carbonation to $CaCO_3$.

Received 19th August 2020,
Accepted 15th October 2020

DOI: 10.1039/d0cp04410e

rsc.li/pccp

Introduction

The continuous global economic growth results in a constant increase in the energy demand. Currently, over 80% of the total primary energy supply is derived from fossil fuels, *i.e.* coal, oil and natural gas.[1] The combustion of fossil fuels releases large volumes of CO_2 into the atmosphere which in turn is most likely linked to global warming.[2] Besides energy saving strategies and the transition to renewable energy carriers, CO_2 capture and storage (CCS) is expected to provide an appreciable contribution to the global reduction targets in CO_2 emissions. Currently, the only industrially available CO_2 capture technology is amine scrubbing.[3] However, amine scrubbing is expensive and associated with the formation of hazardous by-products such as nitrosamines.[4,5] Therefore, alternative CCS technologies are currently explored, with calcium looping (CaL) being one of the most promising candidates. CaL is based on the reversible carbonation–calcination reaction pair

$$CaO\ (s) + CO_2\ (g) \leftrightarrow CaCO_3\ (s),\ \Delta H^0_{298K} = \pm 178\ kJ\ mol^{-1}$$

and stands out due to the very high theoretical CO_2 uptake capacity of CaO (0.78 $g_{CO_2}\ g_{sorbent}^{-1}$), low predicted CO_2 capture costs (*ca.* 23.7 USD $t_{CO_2}^{-1}$)[6] and the high abundance and inexpensiveness of naturally-occurring CaO precursors, *e.g.* limestone.[7] However, the Tammann temperature of $CaCO_3$ (T_T = 533 °C), which is lower than the operating temperatures of the process (600–950 °C), is a major drawback of CaL. The low Tammann temperature results in material sintering and the loss of pore volume, which in turn leads to lower CO_2 uptakes.[8–10] To yield a high CO_2 uptake, a CaO-based CO_2 sorbent requires a high pore volume in the micro- and mesoporous range as the molar volume of the product, $CaCO_3$, is approximately twice as high as that of CaO.[7] Several material design strategies have been proposed to reduce the sintering-induced material deactivation, such as the stabilization of CaO with high-T_T materials (*e.g.* Al_2O_3 or MgO)[7,11–17] or the addition of alkali metal salts.[18–23] Currently, there is very limited understanding of the effect of the addition of alkali metal salts on the CO_2 capture performance of CaO; indeed, several works have reported conflicting results.[18–21] For example, it has been reported that the addition of alkali metal chlorides and hydroxides (with the exception of Li-based salts) strongly increases the CO_2 uptake capacity of CaO, although no

[a] *ETH Zürich, Laboratory of Energy Science and Engineering, Leonhardstrasse 21, CH 8092 Zürich, Switzerland. E-mail: abdalap@ethz.ch, muelchri@ethz.ch*
[b] *PSI, SLS, 5232 Villigen, Switzerland*

† Electronic supplementary information (ESI) available. See DOI: 10.1039/d0cp04410e

cyclic stability data was reported.[18] A further study confirmed the positive effect of the addition of NaCl and, to a lesser extent of Na_2CO_3, on the CO_2 uptake of limestone-derived CaO when tested in a thermogravimetric analyzer (TGA); yet a negative effect was observed when the cyclic CO_2 capture tests were performed in a laboratory-scale fluidized bed.[19] Further, a significant drop in the CO_2 uptake of limestone was observed when Na_2CO_3 was added.[20] Upon the addition of Na_2CO_3, the double carbonate $Na_2Ca(CO_3)_2$ can form under reaction conditions.[22,23] The formation of $Na_2Ca(CO_3)_2$ has been linked to an increase in the kinetics of both the carbonation and calcination reactions and an increased cyclic stability of the sorbent when compared to pristine CaO.[22,23]

Recent work has explored the effect of the addition of the double salt $(Li\text{-}K)_2CO_3$ to CaO on its CO_2 uptake.[21] After 23 carbonation/calcination cycles a three times higher CO_2 uptake was observed when compared to pure CaO.[21] It was speculated that the addition of $(Li\text{-}K)_2CO_3$ prevents the formation of a $CaCO_3$ layer that would otherwise impose a high diffusion resistance for CO_2, thus providing a direct access for CO_2 to unreacted CaO. However, a limitation of the studies described above is that the cyclic CO_2 uptake of alkali metal salt-promoted CaO was determined under mild reaction conditions that are of little relevance for practical use, *i.e.* the calcination step was performed in pure N_2 at $T \leq 850$ °C. Furthermore, there has been very little insight into the morphological and structural modifications that arise from the addition of alkali metal salt promoters. Hence, in this work we study in detail the effect of the addition of the alkali salt Na_2CO_3 on the CO_2 uptake of CaO under industrially relevant conditions. The CO_2 uptake performance of sorbents is complemented by a detailed characterization of the alkali metal salt-induced structural and morphological changes of the sorbent using a combination of electron microscopy and X-ray absorption spectroscopy (XAS). These experiments allowed us to link the sorbents' decreasing CO_2 uptake to sintering that is induced by the formation of the low melting point double carbonate $Na_2Ca(CO_3)_2$. Furthermore, $Na_2Ca(CO_3)_2$ was found to be stable under both carbonation and calcination conditions and to cover the surface of unreacted CaO preventing in turn the carbonation reaction to proceed rapidly.

Experimental

Material preparation

Commercial $CaCO_3$ (Fischer Chemicals, CAS: 471-34-1, analytical reagent grade) and Na_2CO_3 (Acros Organics, CAS: 497-19-8, 99.5% purity) were used for the synthesis of the CO_2 sorbents (Fig. S1, ESI†). To achieve a homogeneous distribution of the sodium salt modifier, a wet ball-milling technique following a reported method was employed.[14] Specifically, 7 g of the precursor powders, mixed with 10 mL of deionized water, were ball-milled in a 45 mL Si_3N_4 jar containing 5 mm Si_3N_4 balls. The ball-milling time was 48 h at 500 rpm. After ball milling, the suspension obtained was dried in an oven overnight at 100 °C. The following nomenclature is used for the samples: Ca/*x*Na, whereby *x* refers to the quantity of Na_2CO_3 (wt%). The following values for *x* were used: 1, 3, 6, 10 and 20 wt%. Pure ball-milled $CaCO_3$ was used as the reference material for the CO_2 uptake experiments (referred to as Ca/0Na).

The reference $Na_2Ca(CO_3)_2$ material was synthesized from a stoichiometric mixture of Na_2CO_3 and $CaCO_3$ at 800 °C in a CO_2 atmosphere for 2 h.

Materials characterization

The mass ratio of Na : Ca in the sorbents was determined by inductively coupled plasma optical emission spectroscopy (ICP-OES) using an Agilent 5100 VDV instrument; the samples were digested in aqua regia.

The crystallinity and phase composition of the sorbents were analyzed by X-ray powder diffraction (XRD). The XRD data were collected using a PANalytical Empyrean X-ray diffractometer equipped with a Bragg–Brentano HD mirror, which was operated at 45 kV and 40 mA using CuKα radiation (λ = 1.54 Å). The materials were examined within the 2θ range of 5–90° using a step size of 0.0167°. The scan time per step was 1 s.

N_2 physisorption (Quantachrome NOVA 4000e) was used to determine the surface area and pore volume of the CO_2 sorbents in both the as-prepared and calcined states. Prior to the measurements, all samples were degassed at 300 °C for at least 2 h. The Brunauer–Emmett–Teller (BET)[24] and the Barrett–Joyner–Halenda (BJH)[25] models were used to calculate the surface area and pore volume, respectively.

The particle size and morphology of the CO_2 sorbents synthesized was examined using scanning electron microscopy (SEM). SEM was performed on a LEO Gemini 1530 (Zeiss, Germany) at 5 kV acceleration voltage. Prior to imaging, all samples were sputtered with a thin (*ca.* 3 nm) layer of Pt. Energy-dispersive X-ray spectroscopy (EDX) mapping was obtained at 20 kV acceleration voltage on samples without a Pt coating. Cross-sections of the synthesized materials were prepared by focused ion beam (FIB) equipped with a Ga ion source and imaged with a high-resolution FE-SEM (Zeiss, FIB-SEM NVision 40). For elemental mapping, an Edax EDX detector was used.

X-ray absorption spectroscopy (XAS) experiments were performed at the Phoenix Beamlines (X07MA/B) at the Swiss Light Source (SLS, PSI, Villigen, Switzerland). Data were collected in fluorescence mode (Vortex four-element Si-drift diode detector). For the reference materials, total electron yield signals were also acquired and compared to the fluorescence-detected data to account for self-absorption. The incident intensity I_0 was measured as the total electron yield signal using a 0.5 μm thin polyester foil coated with Ni. All XAS measurements were performed in a vacuum chamber (*ca.* 2.5×10^{-5} mbar) using materials supported on a copper plate, while metallic indium was used for sample fixation. The data were acquired in the range of 950–1600 eV and 3900–4800 eV for the Na and Ca K-edges, respectively. XAS data processing was performed using the Athena software (Demeter 0.9.25 software package).[26] Energy calibration was performed using NaCl (1075.6 eV at the inflexion point).[27]

CO_2 capture test

The materials synthesized were first assessed with regards to their CO_2 uptake performance in a TGA (Mettler Toledo TGA/DSC 3).

In a typical TGA experiment 10–14 mg of sample was placed in a 900 μL sapphire crucible. Prior to the cyclic CO_2 uptake experiments, all samples were calcined at 800 °C for 2 h in N_2. The carbonation reaction was performed for 20 min in 125 cm^3 min^{-1} using 20 vol% CO_2 in N_2 at 650 °C (including a purge flow of 25 cm^3 min^{-1} of N_2 over the microbalance; total flow rate: 150 cm^3 min^{-1}, measured at ambient temperature and pressure). Subsequently, the materials were calcined for 10 min at 900 °C in 30 cm^3 min^{-1} of CO_2 (while maintaining a mandatory purge flow of 25 cm^3 min^{-1} of N_2 over the microbalance). This condition is referred to as CO_2-rich atmosphere. All heating and cooling steps were performed at a rate of 50 °C min^{-1} in either a CO_2-rich atmosphere or 20 vol% CO_2. The carbonation-calcination cycle was repeated 10 times in each experiment. The cyclic CO_2 uptake, expressed in g_{CO_2} $g_{sorbent}^{-1}$, was calculated from the measured weight change as:

$$CO_2 \text{ uptake} = \frac{m_{carb} - m_{calc}}{m_{calc}}$$

where m_{carb} is the sample mass measured at the end of the carbonation stage and m_{calc} is the sample mass measured at the end of the calcination stage. Replacing m_{carb} with $m(t)$, the sample mass measured during the carbonation reaction, gives a CO_2 uptake as a function of time t.

Temperature-programmed carbonation/calcination (TPC) experiments were performed as follows. After an initial calcination step (800 °C, 2 h, N_2) the sample was cooled down to 50 °C in N_2. Next, the sample was heated up from 50 °C to 1000 °C at a rate of 10 °C min^{-1} in a flow of 20 vol% CO_2 in N_2 (total flow rate: 150 cm^3 min^{-1}).

Results and discussion

Synthesis and structural characterization of the as-prepared sorbents

A series of $CaCO_3$–Na_2CO_3 materials with Na_2CO_3 loadings ranging from 1 to 20 wt% were synthesized *via* a wet ball-milling route (Ca/*x*Na, where *x* is the wt% of Na_2CO_3 added, Table S1, ESI†).[14] X-ray powder diffraction (XRD) analysis of the as-prepared (ball-milled) materials revealed only Bragg peaks due to the $CaCO_3$ calcite phase ($R\bar{3}c$ space group) when the Na_2CO_3 loading was below 10 wt% (*e.g.*, Ca/3Na). No crystalline phase of Na_2CO_3 was detected, likely due to the low Na_2CO_3 content and/or its amorphous nature (Fig. 1a and Fig. S2, ESI†). The XRD patterns of materials with higher Na_2CO_3 loading, *i.e.* Ca/10Na and Ca/20Na, showed peaks due to both calcite and Na_2CO_3 ($C2/m$ space group) (Fig. 1a and Fig. S2, ESI†). Scanning electron microscopy (SEM, Fig. S3) analysis of the ball-milled materials showed that the addition of Na_2CO_3 to the sorbents did not have any appreciable influence on the morphology of the materials. For instance, after ball milling, Ca/3Na consisted of submicrometer-sized particles with a particle size comparable to that of Ca/0Na, *i.e.* 0.35 ± 0.15 μm (Fig. S3 and S4, ESI†). Energy-dispersive X-ray spectroscopy (EDX) analysis confirmed a uniform distribution of Na (Na_2CO_3) within the material, as the elemental maps of Ca and Na overlapped with each other and no Na-rich agglomerates were observed (Fig. S4, ESI†). N_2 physisorption analysis revealed that regardless of the sodium content, the sorbents possessed BET surface areas in the range of 9–11 m^2 g^{-1} and BJH pore volumes in the range of 0.04–0.06 cm^3 g^{-1} (Fig. S5, ESI†).

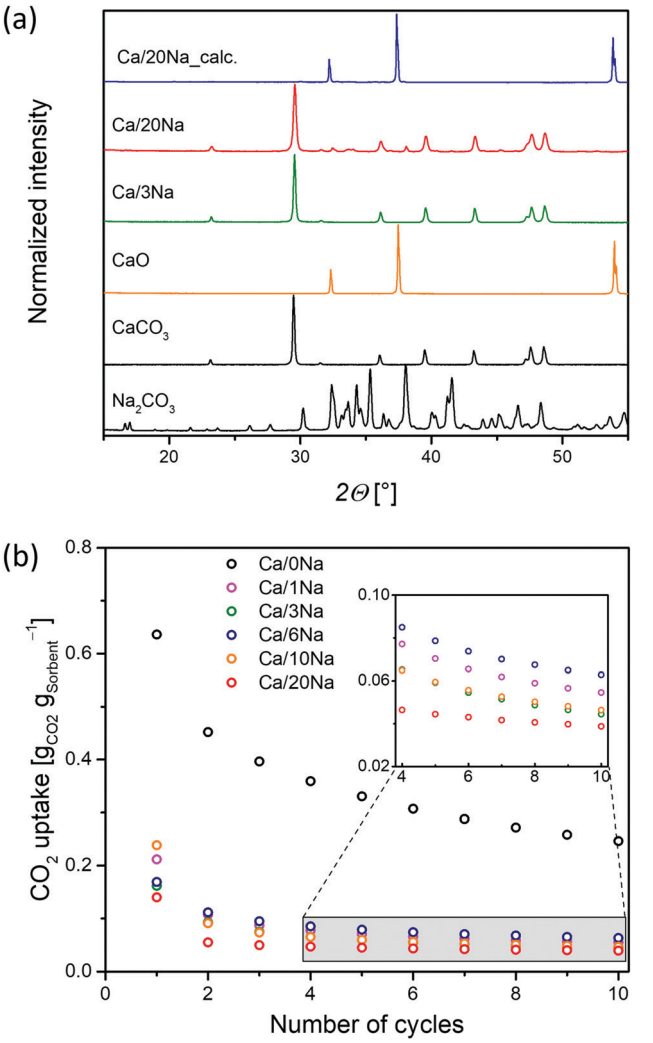

Fig. 1 (a) XRD patterns of CaO-based sorbents as prepared and calcined and Na_2CO_3 and $CaCO_3$ references; (b) cyclic CO_2 capture performance of ball-milled Ca/*x*Na (calcination at 900 °C in CO_2-rich atmosphere; carbonation at 650 °C in 20 vol% CO_2).

Cyclic CO_2 uptake

The cyclic CO_2 uptake performance of the ball-mill derived Ca/*x*Na materials (Fig. 1b) was determined under gas atmospheres and temperatures close to that prevailing in the envisioned large-scale CaL process, *i.e.* the calcination step was performed at 900 °C in a CO_2-rich atmosphere; and the carbonation at 650 °C in 20 vol% CO_2 in N_2. Ca/0Na (*i.e.* the pure ball-milled calcite) exhibited a relatively high initial CO_2 uptake (0.65 g_{CO_2} $g_{sorbent}^{-1}$), however, its CO_2 uptake gradually decreased with cycle number and reached 0.29 g_{CO_2} $g_{sorbent}^{-1}$ after 10 carbonation/calcination cycles. The decay in the CO_2 capacity of unsupported CaO is due to the sintering-induced loss in pore volume owing to the low T_T of $CaCO_3$ of 533 °C.[7] We observed that the addition of Na_2CO_3

to CaO (Ca/*x*Na, with x = 1, 3, 6 10 and 20) led to a dramatic drop in the CO_2 uptake of the sorbents (Fig. 1b) when compared to pure CaO (Ca/0Na). For instance, the maximum CO_2 uptake of Ca/1Na in the 1st cycle was only 0.21 g_{CO_2} $g_{sorbent}^{-1}$, a value that is *ca.* three times lower compared to Ca/0Na (0.65 g_{CO_2} $g_{sorbent}^{-1}$). After the 10th cycle, Ca/1Na showed a CO_2 uptake of 0.05 g_{CO_2} $g_{sorbent}^{-1}$, a value that is *ca.* six times lower compared to Ca/0Na. Increasing the Na_2CO_3 content deteriorated further the CO_2 uptake of the sorbents; for example, Ca/20Na showed CO_2 uptakes of 0.14 g_{CO_2} $g_{sorbent}^{-1}$ and 0.04 g_{CO_2} $g_{sorbent}^{-1}$ in the 1st and 10th cycle, respectively.

Analysis of the temporally-resolved CO_2 uptake curves (Fig. S6, ESI†) revealed an irreversible mass gain Δm after the calcination step (900 °C, CO_2-rich atmosphere) for the Na_2CO_3-modified sorbents. The observed weight gain Δm indicates the incomplete regeneration of $CaCO_3$ to CaO in the calcination step. On the other hand, the CO_2 uptake curve of Ca/0Na showed no weight difference when calcined at 900 °C in a CO_2-rich atmosphere (and in the initial calcination at 800 °C in N_2). Moreover, the values of Δm determined are proportional to the Na content in the materials (Fig. S6, ESI†). This observation suggests the formation of a phase (*i.e.* a Ca–Na mixed phase) that does neither capture nor release CO_2 under the conditions investigated. Further details about the presence and the nature of this phase is provided by SEM and Na K-edge XANES analyses (*vide infra*).

Additionally, temperature-programed carbonation/calcination experiments (TPC, 150 cm^3 min^{-1}, 20 vol% CO_2 in N_2, 50 to 1000 °C, 10 °C min^{-1}) of Ca/0Na, Ca/1Na and Ca/20Na as well as the reference Na_2CO_3 were performed in a TGA (Fig. S7, ESI†). As expected, pure Na_2CO_3 showed no weight increase over the entire temperature range probed. At temperatures above 850 °C, *i.e.* temperatures exceeding the melting temperature of Na_2CO_3 (melting temperature, T_M = 851 °C) a gradual weight loss was detected. This weigh loss was due to the slow decomposition of Na_2CO_3 into Na_2O and CO_2, in agreement with previous observations.[28] Turning to Ca/0Na, the TPC experiment showed a broad peak of weight gain with a maximum at *ca.* 570 °C due to the carbonation of CaO. The weight increase was followed by a rapid weight loss due to the decomposition of $CaCO_3$ starting at 800 °C. Interestingly, the addition of Na_2CO_3 to CaO changed dramatically the sorbent's TPC curve profile. The Na_2CO_3-modified sorbents showed a lower CO_2 uptake at intermediate temperatures (T < 700 °C), while the onset temperature for carbonation was not affected by the addition of Na_2CO_3 (Fig. S7, ESI†). The broad shoulder at intermediate temperatures was followed first by a narrow, sharp peak at $T \approx$ 750 °C, and secondly by a weight loss corresponding to the decomposition of $CaCO_3$. Increasing the Na_2CO_3 content shifted the maximum of the carbonation peak towards higher temperatures, *i.e.* 770 °C for Ca/1Na and 785 °C for Ca/20Na (Fig. S7, ESI†). In contrast to pure Na_2CO_3, the Na_2CO_3-modified sorbents showed no weight loss at high temperatures, indicating the absence of Na_2CO_3 decomposition. We hypothesize that this was due to the formation of a stable Ca–Na mixed phase in CO_2-containing atmospheres (*vide infra*).

Morphological characterization of the calcined sorbents

To understand the effect of the addition of Na_2CO_3 on the sorbents' microstructure and sintering characteristics, XRD, SEM and N_2-physisorption experiments were performed on the calcined materials (initial calcination at 800 °C in N_2). After calcination in N_2 at 800 °C, the average particle size remained largely unchanged (0.4 ± 0.1 μm, Fig. 2a and b) in Ca/0Na. We also observed an increase in the surface area and pore volume of Ca/0Na to, respectively, 16 m^2 g^{-1} and 0.13 cm^3 g^{-1}, (compared to 9 m^2 g^{-1} and 0.04 cm^3 g^{-1}, before calcination), which can be explained by the release of CO_2 during the decomposition of $CaCO_3$ to CaO (XRD, Fig. 1a).[29] Different to Ca/0Na, we observed a considerable increase in particle size due to particle coalescence for the Na_2CO_3-modified sorbents (Fig. 2a and c). For example, the particle size of Ca/1Na increased from 350 nm to *ca.* 1.3 μm, accompanied by a drastic decrease in surface area (from 10 to 2 m^2 g^{-1}) and pore volume (from 0.06 to 0.01 cm^3 g^{-1}). These measurements hint to a dramatic collapse of the sorbents' microstructure (Fig. S5, ESI†).

The temperature dependence of the particle size of the sorbents was investigated in more detail and is shown in Fig. 2a and Fig. S8 (ESI†). Sintering of the Na_2CO_3-modified sorbents started at 500 °C and was likely promoted by the addition of Na_2CO_3 (T_M = 851 °C, T_T = 290 °C) that covered the surface of $CaCO_3$ and/or CaO particles (Fig. 2f), thus, accelerating inter-particle coalescence. The XRD analysis of the calcined, Na_2CO_3-modified sorbents showed only Bragg peaks due to CaO (Fig. 1a, Ca/20Na_calc.), possibly due to the amorphous nature of the Na-containing phase.

The effect of sintering on the CO_2 uptake of the pure CaO sorbent

To determine whether sintering (induced by the addition of Na_2CO_3) was the only reason for the appreciably decreased CO_2 uptake performance of the Na_2CO_3-modified sorbents, we performed a series of control experiments. A set of pure $CaCO_3$ sorbents was sintered by annealing them in a CO_2 atmosphere at 750 °C for varying durations. The SEM micrographs as well as the surface area and pore volume measurements of the respective materials are presented in Fig. S9 and S10 (ESI†), respectively, revealing highly sintered materials with specific surface areas and pore volumes below 2 m^2 g^{-1} and 0.02 m^3 g^{-1}, respectively (carbonated samples). However, similar to the as-prepared Ca/0Na and contrary to the Na_2CO_3-modified sorbents, calcination in N_2 yielded a significant increase in both the surface area and pore volume (Fig. S10, ESI†). Additionally, we performed cyclic CO_2 uptake measurements for the sintered sorbents and compared the performance to that of pure and Na_2CO_3-modified CaO (Fig. S11, ESI†). The sintered sorbents exhibited a worse CO_2 uptake performance when compared to Ca/0Na, but they exceeded substantially the CO_2 uptake performance of the Na_2CO_3-modified sorbents. Specifically, the most sintered, but Na_2CO_3-free sorbent that was annealed for 12 h had a CO_2 uptake of 0.15 g_{CO_2} $g_{sorbent}^{-1}$ in the 10th cycle compared to 0.05 g_{CO_2} $g_{sorbent}^{-1}$ for Ca/1Na. These results indicate that

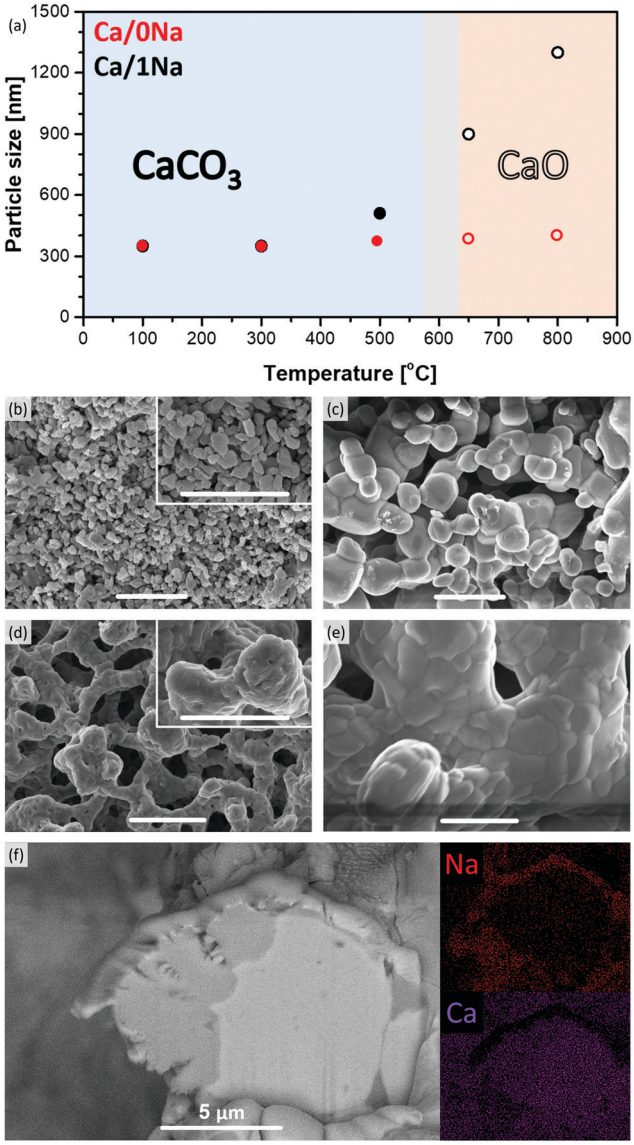

Fig. 2 (a) The evolution of the particle size of Ca/0Na and Ca/1Na during the initial calcination step in N_2, as determined by SEM, as a function of temperature; SEM images of (b) Ca/0Na and (c) Ca/1Na after the first calcination step; and (d) Ca/0Na and (e) Ca/1Na after the 10th carbonation step (the scale bar in (b–e) is equal to 2 μm); (f) cross sectional HR-SEM and EDX elemental mapping of Ca/20Na after the 10th carbonation step.

sintering was one contributor explaining the poor CO_2 uptake of Na_2CO_3-modified CaO, but not the only factor.

Structure and morphology of the cycled sorbents

XRD analysis of cycled Ca/20Na (collected after the carbonation step) revealed that CaO was the major phase with only traces of $CaCO_3$ present. This was in good agreement with the TGA-based CO_2 uptake experiments, where a CO_2 uptake of only 0.04 g_{CO2} $g_{sorbent}^{-1}$ was observed in the 10th cycle, corresponding to a CaO conversion of *ca.* 5%. Additional low-intensity peaks appeared in the diffraction pattern, which are tentatively attributed to the Ca–Na double carbonate $Na_2Ca(CO_3)_2$ phase (in correlation with Na K-edge XAS, *vide infra*). SEM analysis of Ca/1Na after the 10th carbonation cycle (Fig. 2e) revealed an even higher degree of sintering compared to Ca/1Na after the initial calcination and cycled Ca/0Na (Fig. 2c and d, respectively). Despite the drastic, sintering-induced morphological changes, the low magnification SEM/EDX elemental mapping showed no indication of agglomeration of Na-containing phases (*i.e.* the Na maps still revealed a high dispersion of Na over the $CaO/CaCO_3$ particles, Fig. S12, ESI†). To obtain a more detailed insight into the morphology of the material, a cross section of a Ca/20Na particle after the 10th carbonation step was prepared by FIB cutting and analyzed *via* high-resolution SEM/EDX. We observed that the $CaO(CaCO_3)$ particles were covered by a shell of a Na-rich phase (Fig. 2f), while the inner part of the particle was almost free of Na (Fig. 2f).

XAS analysis: the nature of the Na containing phases in the cycled materials

To determine in more detail the nature of the Na-rich phase in the sorbents during the different steps of the CO_2 capture process, Na K-edge XANES data were acquired. After the initial calcination step (800 °C, N_2), the Na K-edge spectra of the sorbents matched perfectly the reference spectra of Na_2CO_3 (Fig. S14, ESI†). This observation, combined with Ca K-edge XAS results (*vide infra*, Fig. S13, ESI†), confirmed that all of the Na_2CO_3-modified sorbents consisted of a mixture of CaO and Na_2CO_3 after the initial calcination step and no Ca–Na mixed phase was present. The Na K-edge XANES spectra of all of the sorbents collected after the 10th carbonation step had a similar profile with a very characteristic shape of the XANES spectrum that was different from the XANES spectrum of pure Na_2CO_3 (Fig. 3). Specifically, all spectra possessed a pre-edge peak at *ca.* 1073.2 eV (−1.5 eV with respect to the absorption edge, feature A, Fig. 3), while Na_2CO_3 possessed a pre-edge feature at *ca.* 1073.5 eV (−1.2 eV with respect to the absorption edge). Additionally, contrary to the spectrum of Na_2CO_3 with a white line maximum at 1078.5 eV, the white line region of the Na_2CO_3-modified sorbents consisted of three defined features, *i.e.* B (*ca.* 1076.3 eV), C (*ca.* 1078 eV) and D (*ca.* 1080.6 eV, maximum intensity of the spectra) (Fig. 3). Notably, the obtained Na K-edge spectra of the Na_2CO_3-modified sorbents did not correspond to any previously reported XANES spectrum of Na-based materials. On the other hand, the spectra matched perfectly the $Na_2Ca(CO_3)_2$ reference ($P2_1ca$ space group,[30] see XRD of the synthesized reference in Fig. S15, ESI†). The Na K-edge XAS spectrum of $Na_2Ca(CO_3)_2$ is shown in Fig. 3 and, to the best of our knowledge, is reported here for the first time. A perfect match between the spectrum of $Na_2Ca(CO_3)_2$ and the spectra of the cycled Na_2CO_3-modified sorbents (collected after the carbonation step) revealed the formation of the Ca–Na double carbonate ($Na_2Ca(CO_3)_2$) under carbonation conditions (Fig. 3). Hence, the Na-rich phase that was observed by cross-sectional FIB-SEM (Fig. 2f) to cover the surface of $CaO/CaCO_3$ particles was $Na_2Ca(CO_3)_2$. Fig. 3 demonstrates that Na K-edge XANES can be used as a fingerprint to distinguish between Na in Na_2CO_3 or $Na_2Ca(CO_3)_2$ environments. Being an element selective technique, XANES allowed us to study the Na environment in the materials,

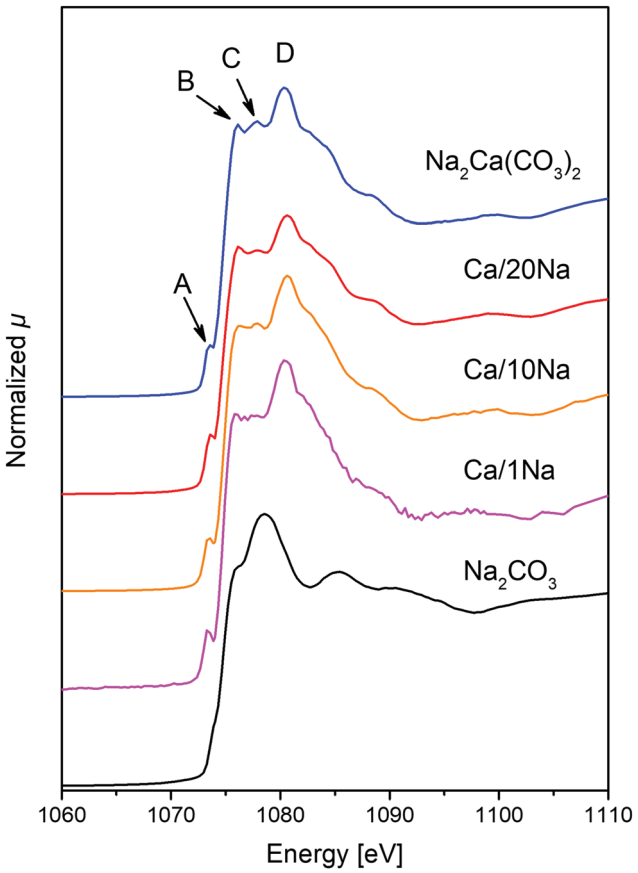

Fig. 3 Na K-edge XANES spectra of Ca/1Na, Ca/10Na and Ca/20Na after 10th carbonation, as well as the references Na_2CO_3 and $Na_2Ca(CO_3)_2$.

even when using relatively low Na contents (*i.e.* < 10 wt% Na_2CO_3); a composition for which XRD failed to provide sufficient information on the Na containing phases.

Na K-edge XAS data were complemented by Ca K-edge XAS of the materials (Fig. S13, ESI†). The spectra of the as-prepared materials matched the reference calcite ($CaCO_3$), revealing that no phase transformation (*e.g.* formation of aragonite $CaCO_3$ polymorph)[14] occurred during the ball-milling process (Fig. S13, ESI†). The spectra of the sorbents after the initial calcination step (800 °C, N_2) matched the reference CaO. For the sample collected after the 10th carbonation cycle, and in line with XRD, the Ca K-edge spectra showed that the Ca was mainly in a CaO environment. Nonetheless, some features corresponding to $CaCO_3$ could also be distinguished. These observations are in line with the TGA CO_2 uptake experiments revealing a CO_2 uptake below 0.05 $g_{CO_2}\ g_{sorbent}^{-1}$ after 10 cycles. Since the majority of the Ca atoms was present in a CaO phase, the Ca K-edge spectra could not distinguish well between the different types of carbonate phases (*i.e.* $CaCO_3$ and $Na_2Ca(CO_3)_2$).

Discussion

After elucidation of the nature of the Ca–Na mixed phase, we carried out a control experiment to evaluate the performance of pure $Na_2Ca(CO_3)_2$ under cyclic carbonation-calcination conditions (Fig. S16, ESI†). It was found that in the initial calcination in pure N_2 $Na_2Ca(CO_3)_2$ decomposed into CaO and Na_2CO_3 (at *ca.* 600 °C, as determined from the weight loss). In the following carbonation step a rapid weight gain was observed. No weight change was detected during the subsequent calcination step, confirming the stability of $Na_2Ca(CO_3)_2$ during calcination at 900 °C in a CO_2-rich atmosphere (Fig. S16, ESI†). This observation correlates well with the cyclic carbonation-calcination experiments of Ca/*x*Na as described above. In particular, the observed weight gain Δm by TGA under CO_2 rich atmosphere with respect to the initial calcination step in N_2 (Fig. S6, ESI†) can be explained by the formation of a $Na_2Ca(CO_3)_2$ phase as revealed by XAS that was stable under both carbonation and calcination (in CO_2 rich atmosphere) conditions. Such a weight increase was due to the reaction between CaO, Na_2CO_3 and CO_2 forming $Na_2Ca(CO_3)_2$. The melting point of $Na_2Ca(CO_3)_2$ has been reported as $T_m = 817$ °C,[31] which is significantly lower than the calcination temperature used here (900 °C). Therefore, during calcination (performed in a CO_2-rich atmosphere) the Na_2CO_3-modified sorbent consisted of solid CaO covered by a molten $Na_2Ca(CO_3)_2$ layer. Therefore, the presence of a molten salt layer promoted the sintering of the material.

Overall, based on the results obtained here, the formation of $Na_2Ca(CO_3)_2$ resulted in a dramatic reduction of the CO_2 uptake performance of Na_2CO_3-modified CaO. This negative effect was attributed to (i) the formation of a molten $Na_2Ca(CO_3)_2$ layer during calcination in CO_2 rich atmosphere that promoted sintering, and (ii) the solidification of $Na_2Ca(CO_3)_2$ during carbonation that resulted in a dense layer covering the unreacted (or partially reacted) CaO particles, thus hindering the further carbonation of CaO. Additionally, due to its low Tammann temperature ($T_T \approx 270$ °C), $Na_2Ca(CO_3)_2$ further promoted the sintering of the CaO/$CaCO_3$ particles.

Conclusions

To conclude, we demonstrated that the addition of 1 to 20 wt% Na_2CO_3 to CaO reduces dramatically the CO_2 uptake performance of CaO from *ca.* 0.3 $g_{CO_2}\ g_{sorbent}^{-1}$ for pure CaO to 0.05 $g_{CO_2}\ g_{sorbent}^{-1}$ for Na_2CO_3 modified CaO after ten carbonation cycles. Combining TGA, XAS and FIB-SEM analyses allowed us to assign the formation of $Na_2Ca(CO_3)_2$ as a key factor to explain the poor CO_2 capture performance of Na_2CO_3-modified CaO. The poor CO_2 capture performance of these materials is attributed to the presence of the low Tammann temperature phase $Na_2Ca(CO_3)_2$ that is molten during the calcination step, thereby promoting sintering. During carbonation, a solid, dense layer of $Na_2Ca(CO_3)_2$ covers the unreacted CaO particles, thus preventing its carbonation to $CaCO_3$.

Conflicts of interest

The authors declare that there is no conflict of interest regarding the publication of this article.

Acknowledgements

The authors thank ScopeM for the use of their electron microscopy facilities. The Swiss Light Source (SLS, PSI, Villigen), through proposal 20160628, is acknowledged for provision of beamtime. Dr Felix Donat (ETH Zürich) is acknowledged for performing the ICP analyses and for his insightful comments. This project has received funding from the European Research Council (ERC) under the European Union's Horizon 2020 research and innovation programme grant agreement No. 819573. The Swiss National Science Foundation (SNSF, 200020_156015) is acknowledged for partial financial support.

References

1 World Energy Balances 2019, IEA, Paris, 2019.
2 R. A. Betts, O. Boucher, M. Collins, P. M. Cox, P. D. Falloon, N. Gedney, D. L. Hemming, C. Huntingford, C. D. Jones, D. M. H. Sexton and M. J. Webb, *Nature*, 2007, **448**, 1037–1041.
3 G. T. Rochelle, *Science*, 2009, **325**, 1652–1654.
4 K. Veltman, B. Singh and E. G. Hertwich, *Environ. Sci. Technol.*, 2010, **44**, 1496–1502.
5 N. A. Fine, P. T. Nielsen and G. T. Rochelle, *Environ. Sci. Technol.*, 2014, **48**, 5996–6002.
6 A. MacKenzie, D. L. Granatstein, E. J. Anthony and J. C. Abanades, *Energy Fuels*, 2007, **21**, 920–926.
7 A. M. Kierzkowska, R. Pacciani and C. R. Muller, *ChemSusChem*, 2013, **6**, 1130–1148.
8 J. C. Abanades and D. Alvarez, *Energy Fuels*, 2003, **17**, 308–315.
9 G. S. Grasa and J. C. Abanades, *Ind. Eng. Chem. Res.*, 2006, **45**, 8846–8851.
10 P. Sun, J. R. Grace, C. J. Lim and E. J. Anthony, *AIChE J.*, 2007, **53**, 2432–2442.
11 H. Lu, A. Khan, S. E. Pratsinis and P. G. Smirniotis, *Energy Fuels*, 2009, **23**, 1093–1100.
12 M. Broda and C. R. Muller, *Adv. Mater.*, 2012, **24**, 3059–3064.
13 W. Liu, H. An, C. Qin, J. Yin, G. Wang, B. Feng and M. Xu, *Energy Fuels*, 2012, **26**, 2751–2767.
14 A. Kurlov, M. Broda, D. Hosseini, S. J. Mitchell, J. Perez-Ramirez and C. R. Muller, *ChemSusChem*, 2016, **9**, 2380–2390.
15 A. Armutlulu, M. A. Naeem, H. J. Liu, S. M. Kim, A. Kierzkowska, A. Fedorov and C. R. Muller, *Adv. Mater.*, 2017, **29**, 1702896.
16 R. Han, J. Gao, S. Wei, Y. Su and Y. Qin, *J. Mater. Chem. A*, 2018, **6**, 3462–3470.
17 C. Ping, B.-Q. Feng, Y.-L. Teng, H.-Q. Chen, S.-L. Liu, Y.-L. Tai, H.-N. Liu and B.-X. Dong, *RSC Adv.*, 2020, **10**, 21509–21516.
18 E. P. Reddy and P. G. Smirniotis, *J. Phys. Chem. B*, 2004, **108**, 7794–7800.
19 C. Salvador, D. Lu, E. J. Anthony and J. C. Abanades, *Chem. Eng. J.*, 2003, **96**, 187–195.
20 V. Manovic, E. J. Anthony, G. Grasa and J. C. Abanades, *Energy Fuels*, 2008, **22**, 3258–3264.
21 L. Huang, Y. Zhang, W. Gao, T. Harada, Q. Qin, Q. Zheng, T. A. Hatton and Q. Wang, *Energy Technol.*, 2017, **5**, 1328–1336.
22 A. Al-Mamoori, H. Thakkar, X. Li, A. A. Rownaghi and F. Rezaei, *Ind. Eng. Chem. Res.*, 2017, **56**, 8292–8300.
23 C. H. Lee, S. W. Choi, H. J. Yoon, H. J. Kwon, H. C. Lee, S. G. Jeon and K. B. Lee, *Chem. Eng. J.*, 2018, **352**, 103–109.
24 S. Brunauer, P. H. Emmett and E. Teller, *J. Am. Chem. Soc.*, 1938, **60**, 309–319.
25 E. P. Barrett, L. G. Joyner and P. P. Halenda, *J. Am. Chem. Soc.*, 1951, **73**, 373–380.
26 B. Ravel and M. Newville, *J. Synchrotron Radiat.*, 2005, **12**, 537–541.
27 R. J. Prado and A. M. Flank, *Phys. Scr.*, 2005, **T115**, 165–167.
28 J.-W. Kim and H.-G. Lee, *Metall. Mater. Trans. B*, 2001, **32**, 17–24.
29 R. Barker, *J. Appl. Chem. Biotechnol.*, 1973, **23**, 733–742.
30 P. N. Gavryushkin, V. G. Thomas, N. B. Bolotina, V. V. Bakakin, A. V. Golovin, Y. V. Seryotkin, D. A. Fursenko and K. D. Litasov, *Cryst. Growth Des.*, 2016, **16**, 1893–1902.
31 R. H. Mitchell and B. A. Kjarsgaard, *Can. Mineral.*, 2008, **46**, 971–980.